POLITECNICO DI TORINO
Repository ISTITUZIONALE

Torino e la Fabbrica di Cioccolato (Turin and the Chocolate Factory)

Original
Torino e la Fabbrica di Cioccolato (Turin and the Chocolate Factory) / Sparavigna, A.C.. - ELETTRONICO. - (2024). [10.5281/zenodo.11003740]

Availability:
This version is available at: 11583/3011887 since: 2026-06-11T06:13:52Z

Publisher:

Published
DOI:10.5281/zenodo.11003740

Terms of use:

This article is made available under terms and conditions as specified in the corresponding bibliographic description in the repository

Publisher copyright

(Article begins on next page)

26 November 2026

Sizing and Economic Assessment for Auxiliar Components and Grid Connection of a MgB_2-LH_2 Hybrid Power Cable

Giovanni Mangiulli, Michela Bracco, Marco Breschi, *Senior Member, IEEE*, Lorenzo Cavallucci, *Member, IEEE*, Stefania Farinon, Antonio Macchiagodena, Riccardo Musenich, and Laura Savoldi, *Senior Member, IEEE*

***Abstract*—The successful integration in the transportation of two very different commodities, namely electricity and liquid hydrogen LH2, in hybrid cables requires several auxiliary components, including storage tanks for hydrogen before and after terminal points, current leads designed for the efficient coupling and decoupling of current-cryogen flow within the transmission line, a pumping system to ensure the effective circulation of the cryogenic fluid and grid connections from the electric power production plant to the grid through the superconducting cable. These components significantly impact on the overall cost structure and are crucial for the potential market adoption of the technology. This study focuses the dimensioning of the auxiliary components through an evaluation of their thermal-hydraulic parameters, followed by an assessment of their effects on overall costs and economic viability. The reference case study is a 30 km-long MgB2 cable, capable of transmitting 10 kA at 30 kV of voltage, cooled by 20 K-liquid hydrogen. This provides essential insights into the potential scalability and sustainability of the proposed system.**

***Index Terms*—Cryogenics, hydrogen storage, cooling, power cables, cost analysis, superconductivity.**

Received 13 October 2025; revised 18 December 2025; accepted 27 December 2025. Date of publication 5 January 2026; date of current version 23 January 2026. This work was supported by the Ministero dell'Università e della Ricerca within the PRIN 2022 Program under Grant D.D.104 -02/02/2022. *(Corresponding author: Giovanni Mangiulli.)*

Giovanni Mangiulli is with the MAHTEP Group, Dipartimento Energia "Galileo Ferraris", Politecnico di Torino, I-10129 Torino, Italy (e-mail: giovanni.mangiulli@polito.it).

Michela Bracco is with the MAHTEP Group, Dipartimento Energia "Galileo Ferraris", Politecnico di Torino, 10129 Torino, Italy, also with the Istituto Nazionale di Fisica Nucleare, sez. di Genova, 16146 Genova, Italy, and also with the Department of Physics, Università degli Studi di Genova, I-16146 Genova, Italy (e-mail: michela.bracco@ge.infn.it).

Marco Breschi, Lorenzo Cavallucci, and Antonio Macchiagodena are with the Department of Electrical Electronic and Information Engineering, Università degli Studi di Bologna, I-40126 Bologna, Italy (e-mail: marco.breschi@unibo.it; lorenzo.cavallucci@unibo.it; antoni.macchiagoden2@unibo.it).

Stefania Farinon and Riccardo Musenich are with the Istituto Nazionale di Fisica Nucleare, sez. di Genova, 16146 Genova, Italy (e-mail: stefania.farinon@ge.infn.it; riccardo.musenich@ge.infn.it).

Laura Savoldi is with the MAHTEP Group, Dipartimento Energia "Galileo Ferraris," Politecnico di Torino, I-10138 Torino, Italy, and also with the Istituto Nazionale di Fisica Nucleare, sez. di Genova, 16146 Genova, Italy (e-mail: laura.savoldi@polito.it).

Color versions of one or more figures in this article are available at https://doi.org/10.1109/TASC.2026.3651232.

Digital Object Identifier 10.1109/TASC.2026.3651232

I. Introduction

SUPERCONDUCTING power cables (HTS) are a promising lever for grid decarbonization because—under cryogenic operation—they can carry high currents with negligible resistive losses., whereas conventional transmission and distribution exhibit Joule losses on the order of ∼6% of delivered electricity [1], which implies additional generation and associated CO_2 emissions. The main barrier to large-scale HTS adoption is the cost and complexity of sustaining cryogenic conditions. This penalty can be mitigated when the coolant is itself a tradable commodity: using liquid hydrogen as the refrigerant allows the refrigeration duty to be embedded in the hydrogen value chain, enabling the co-delivery of electricity and LH_2 and improving overall techno-economics [2]. Such technologies can be framed as Superconducting Energy Pipelines (SCEP), also referred to as hybrid cables. Programs such as SCARLET [3] aim to demonstrate system-level feasibility and encourage large-scale construction and design of hybrid cables [4]. Among available HTS options, MgB_2 is the most compatible with liquid hydrogen, owing to its critical temperature $T_c \approx 39$ K [5] and comparatively low cost; it is therefore well matched to a LH_2 supply temperatures (∼20 K). As a recent case study, we consider a submarine 30 km-long hybrid cable rated at 300 MW off-shore plant (with a transport current of 10 kA at a voltage of 30 kV) that co-transports hydrogen at ∼1 kg/s (Fig. 1) [4]. In this SCEP layout, a set of concentric flexible cryostats provides the hydrogen flow path, ensures thermal insulation for both fluid and cable, and protects the cable from the external environment. In the layout, several auxiliary subsystems are identified, each essential to reliable operation: current leads, enabling the transfer of electrical current from ambient to cryogenic temperature; a LH_2 pump to circulate the refrigerant through the cryostat; storage tanks to buffer and manage the hydrogen delivered to the network; grid interfaces providing electrical connection from the power-generation plant to the external grid.

The focus of the present work is the dimensioning of these auxiliary components, together with an economic evaluation for each one of them. The auxiliary *cryogenic* SCEP components considered in this study include the upstream and downstream storage tanks, the liquid hydrogen pumping system, and the two current leads required for the electrical connection at the inlet

© 2026 The Authors. This work is licensed under a Creative Commons Attribution 4.0 License. For more information, see https://creativecommons.org/licenses/by/4.0/

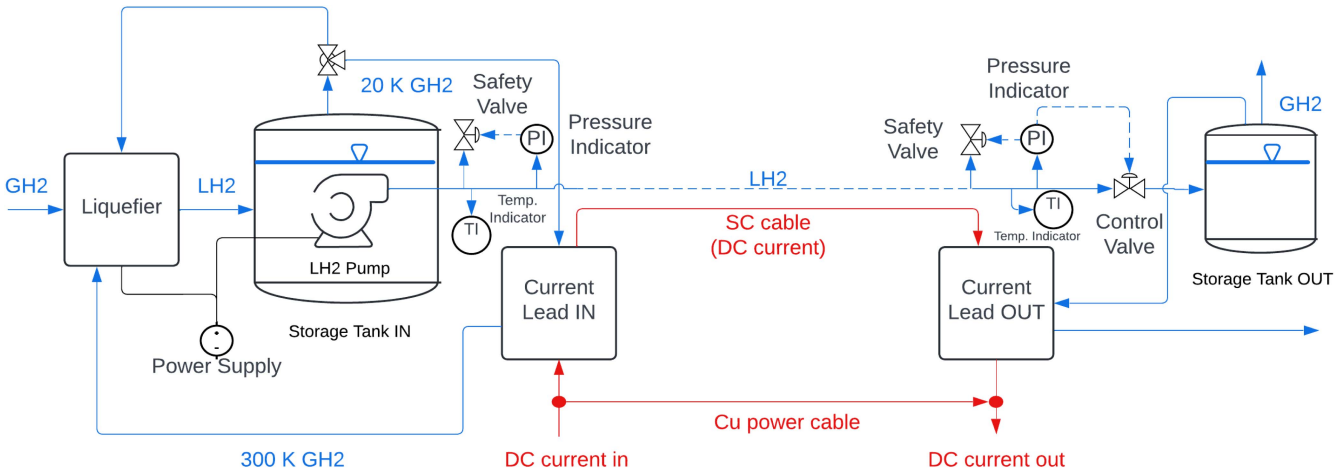

Fig. 1. Layout of the hybrid pipeline, with the auxiliaries for the supply and manage of the cryogen, and the detail of the cable cross section.

and outlet. The pumping system, being strongly dependent on the hydraulic conditions of the hydrogen flow, has not been subjected to a detailed design procedure in the present work; rather, it has been included only in the economic assessment, with costs treated on a qualitative basis. The thermo-hydraulic operating conditions assumed for liquid hydrogen correspond to an inlet temperature of 20 K, with mass flow rates in the range of 0.6–1.4 kg/s and pressures between 7 and 12 bar. On the *electrical* side, the auxiliary components are represented by the interfaces connecting the power generation system to the cable, and the subsequent connection of the cable to the external power grid. Those elements are crucial to ensure a reliable integration of the SCEP into both the production and distribution stages of the energy system. It should be noted that the auxiliary components considered in the present analysis do not include safety systems, as their assessment would require a more detailed study of the possible cable accidents [6], [7].

II. Cryogenic Components Sizing

A. Storage Tanks

Two storage tanks are employed for the collection of hydrogen at the inlet and outlet of the SCEP. The upstream tank receives liquid hydrogen from the liquefier under saturation conditions and, through the submerged cryogenic pump, supplies the refrigerant to the cable (Fig. 2). It also has the function of liquid reservoir, providing additional hydrogen during demand peaks. The downstream tank collects the hydrogen leaving the cable, which is subsequently delivered to the end users. This tank also operates under saturation conditions, corresponding to the outlet temperature, that can be reached via expansion of a downstream valve.

For this sizing process, the number and capacity of upstream storage tanks were determined for each nominal cable mass-flow scenario assuming no hydrogen leakages. In the absence of downstream demand data, the outlet storage was assumed identical to the inlet storage in both tank number and capacity.

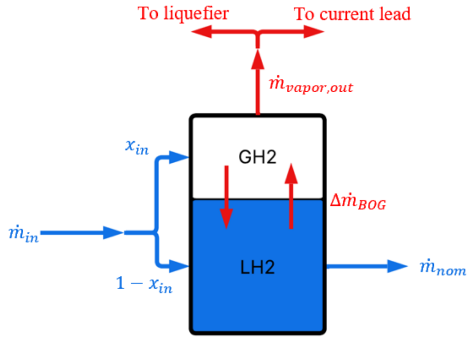

Fig. 2. Inlet tank mass-balance scheme.

The computation has been done by solving numerically two lumped-parameters liquid-phase mass and energy balances (1) and (2) and computing the total liquid hydrogen inventory per tank (3):

$$\frac{dM_l(t)}{dt} = \dot{m}_{in}(t)\cdot(1-x_{in}) - \dot{m}_{nom}(t) - \Delta\dot{m}_{BOG}(t) \tag{1}$$

$$\frac{dU_l(t)}{dt} = \dot{m}_{in}(t)\cdot(1-x_{in}(t))\cdot h_{sat,l}(p_{tank}) - \lambda(p_{tank})\cdot \Delta\dot{m}_{BOG}(t) - \dot{m}_{nom}(t)\cdot h_{pump} + Q_{pump} + N\cdot Q_{in} \tag{2}$$

$$M_{tot} = V_{tot}\cdot\left[\frac{(1-x(t))}{\rho_{sat,\ l}} + \frac{x(t)}{\rho_{sat,\ v}}\right] \tag{3}$$

where M_l is the liquid-phase mass; $\dot{m}_{in}$ is the inlet mass flow rate to the tank from the liquefier; x_{in} is the vapor quality of this mass flow rate; $\dot{m}_{nom}$ is the cable nominal mass flow rate; $\Delta\dot{m}_{BOG}$ is the boil-off rate generated in the tank; U_l is the internal energy; h indicates enthalpy; λ the latent heat of evaporation; Q_{pump} the inlet heat generated by the pumping system; Q_{in} the parasitic heat from the environment; N the number of tanks; V_{tot} the

TABLE I
PARAMETERS FOR THE NUMBER OF TANKS COMPUTATION

Var.	V_{min} $[m^3]$	x_{in} $[-]$	$\dot{m}_{nom}$ $[kg/s]$
Values	[70; 150; 300; 400]	[0.1; 0.3; 0.5]	[0.6; 1; 1.4]

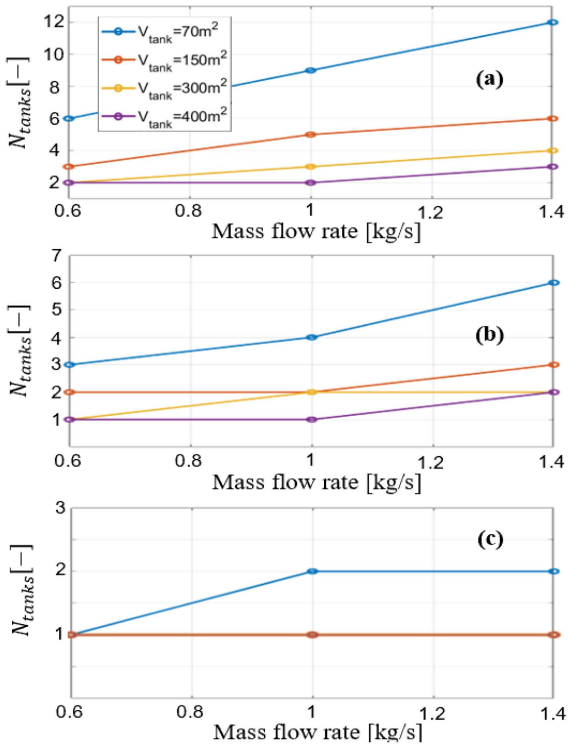

Fig. 3. Tanks required for LF=50% (a); 70% (b) and 90% (c).

volume of the whole tank systems and ρ the density of liquid/vapor. A homogeneous (well-mixed) hydrogen temperature was assumed within the tank—an operating condition that can be promoted by top-entry of the liquefier stream—and a constant boil-off rate was imposed, evaluated at a 50% liquid fill level (LF = 50%) and calculated for a steady state case. An additional design criterion for the inlet tank requires continuous supply for at least 1 h at a peak load equal to +20% of the nominal mass flow ($\dot{m}_{peak} = 1.2\ \dot{m}_{nom}$). Combinations between fixed capacities, inlet hydrogen vapor qualities and nominal mass flow rates of coolant (Table I) produce possible number of tank designs by solving (1) with $\dot{m}_{peak}$.

Among the feasible configurations defined by single-tank volume, tank count, inlet vapor quality, and cable mass-flow rate (Fig. 3, with $L\ F_{t=0} = 1 - x_{in}$ at steady state), the selected solution was chosen based on capital cost, peak-load emptying time, and ground-occupied space. The space criterion was considered due to the space constraint on the offshore platform for the selected case study. The tank bottom area was evaluated assuming vertically axis-oriented cylindrical vessels (commercially prevalent) with an aspect ratio AR = H/D = 2; lower AR generally mitigates thermal stratification, with a

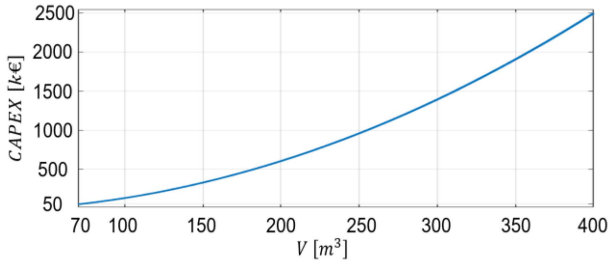

Fig. 4. Cost function per tank size.

TABLE II
OPTIMUM CONFIGURATIONS FOR I/O TANKS ($N_{tanks} = 1$)

$\dot{m}_{nom}\left[\frac{kg}{s}\right]$	V_{tank} $[m^3]$	$S_{floor}[m^2]$	$\tau[h]$	C [M€]	x
0.6	70	9.87	~1.5	0.05	0.1
1	150	16.41	~2	0.3	0.1
1.4	150	16.41	~2	0.3	0.1

sphere corresponding to AR ~ 1 [8], [9]. Emptying times under peak-load conditions were computed from (1). Capital costs were inferred from limited vendor data [10] for 70 and 400 m^3 units by fitting an assumed parabolic cost function and applying it across intermediate capacities (Fig. 4).

For each nominal mass-flow scenario, the configuration selection was formulated as a linear programming problem. The objective is to minimize the plan-view footprint, reflecting the primary constraint of limited space on the offshore platform. The solution must satisfy two operational constraints: the total capital cost $\leq$ 0.5 M€ and the peak-load emptying time $\geq$ 1 h. Optimal configurations for mass-flow scenarios are collected in Table II. Based on the optimization results, a single inlet-storage configuration is optimal for two of the three nominal mass-flow scenarios: $V_{tank} = 150\ m^3$, $N_{tanks} = 1$, CAPEX = 0.30 M€, and inlet vapor quality $x_{in} = 0.1$ which implies a steady-state liquid level of the 90% . Since its occupied surface is comparable with that of the 0.6 kg/s baseline, the same inlet configuration can be adopted for all three operating conditions without violating the cost/time constraints (CAPEX $\leq$0.5 M€; emptying time $\geq$1 h). This standardization simplifies system-level cost analysis; by symmetry, the outlet storage is likewise standardized.

B. Current Leads

Vapor-cooled current leads are integrated with the hydrogen streams available at the upstream and downstream tanks. Upstream, only a small bleed fraction of the saturated vapor is routed through the inlet lead as counter-flow coolant, while the bulk is returned to the liquefier to preserve a low-enthalpy recycle and economize the process [11]. Downstream, the same vapor stream is employed to cool the outlet lead and is subsequently warmed and conditioned to meet end-use requirements (e.g., electrolyzers, alternative-fuel applications). The inlet lead is implemented as a hybrid assembly comprising a warm resistive segment (Cu) near ambient temperature and an intermediate HTS section (REBCO) that bridges to the cable interface temperature

(∼20 K) ahead of the MgB_2 joint [12], [13]. This architecture minimizes cold-end heat inleak, allowing the inlet lead to be cooled with a limited vapor bleed [14]. In contrast, the outlet lead is realized as a fully resistive design: removing an HTS bridge maintains I^2R losses in the whole segment, requiring a larger fraction of the available vapor aiding its intentional warming.

Eqs. (4) and (5) describe the thermal behavior of the current lead [15] and hydrogen vapor at steady state conditions. θ is the current lead temperature while T corresponding to the fluid one, $k(\theta)$ and $\rho(\theta)$ are, respectively, thermal conductivity and electrical resistivity of copper/HTS, $A(x)$ is the section of the solid, I the electrical current through the lead, h the heat transfer coefficient through the solid and fluid, P_w is the wetted perimeter, $c_p(T)$ is the specific heat at constant pressure (assumed as function of temperature only) and $\dot{m}_{H_2}$ is the coolant mass flow rate.

$$\frac{d}{dx}\left[k\left(\theta\right)\cdot A\left(x\right)\cdot\frac{d\theta}{dx}\right]+I^2\cdot\frac{\rho\left(\theta\right)}{A\left(x\right)}=h\cdot P_w\cdot\left(\theta-T\right) \tag{4}$$

$$\dot{m}_{H_2}\cdot c_p\left(T\right)\cdot\frac{dT}{dx}=h\cdot P_w\cdot\left(\theta-T\right) \tag{5}$$

Solutions of these two equations are the thermal profiles of the current lead and the vapor, which depend on the size of the solid and the mass flow rate of the fluid. For different parameters, the optimal current lead configuration can be found for such application by minimizing geometry and/or mass flow rate. For a qualitative design, an ideal heat transfer can be assumed [16] ($h\rightarrow\infty$, $\theta=T$). (4) and (5) become a unique equation, solved with finite differences numerical method, that describes the thermal behavior of the whole system Cu+HTS+H_2 (6):

$$\frac{d}{dx}\left[k\left(T\right)\cdot A\left(x\right)\cdot\frac{dT}{dx}\right]+I^2\cdot\frac{\rho\left(T\right)}{A\left(x\right)}=\dot{m}_{H_2}\cdot c_p\left(T\right)\cdot\frac{dT}{dx}. \tag{6}$$

The equation can be solved imposing $T\left(0\right)=20\,K$, $T\left(L\right)=300\;K$. Considering the inlet current lead the total length L includes an HTS section of length L_{HTS}<L followed by a warm copper segment. The HTS stack comprises REBCO tapes with a copper stabilizer. For heat conduction along $0<x\leq L_{HTS}$, the composite is treated with an area-weighted homogeneous thermal conductivity based on the equivalent cross-sections of copper and tapes, with the tape conductivity is taken from Lu et al. [17].The number of tapes, N_{tapes} , is determined from the temperature profile to meet the required current margin.

Current sharing is enforced locally along the HTS section. If $I/N_{tapes}\leq I_{crit}(T)$ the HTS resistivity is set to zero (no ohmic losses in the tapes). If the condition is violated, the excess current ΔI = I−I_{crit}(T) is carried by the copper stabilizer; the associated I^2R losses are computed using the stabilizer cross-section and the length of the parallel path with respect to the HTS, in this case L_{HTS}. A design current of 15 kA is adopted (rather than the 10 kA case-study value) to account for possible overcurrent events. For x>L_{HTS}, the lead is modelled as copper only. Copper properties (thermal and electrical) are taken from NIST with RRR = 60 [18]; hydrogen thermophysical properties are also taken from NIST [19]. This piecewise formulation captures the HTS–stabilizer composite behaviour near the cold end and the fully resistive behaviour toward the warm end, while preserving a clear check on cold-end heat load and temperature margins. Given (6), a parametric sweep was performed. The model takes as inputs the hydrogen mass flow rate, varied between 0.1 and 5 g/s, and the main geometric descriptors: total lead length L, HTS segment length L_{HTS} , equivalent diameter of the copper segment, and equivalent overall diameter of the HTS stack. From the latter and the computed number of tapes, the copper stabilizer cross-section in the HTS region is obtained by subtracting the total tape area from the HTS equivalent area. For each input combination, the solver produces a candidate current-lead design together with the parasitic heat conducted to the superconducting cable across the cold plate (cold-end heat inleak at ∼20 K) and the associated cost, including CAPEX and OPEX. Fixed costs have been computed just considering HTS tapes (100-150 USD kA-1 m-1) [20], which are the most relevant material contribution. Operating costs, instead, have been estimated considering that the amount of coolant used for current leads must be liquefied again from ambient temperature, which means that it becomes a liquefaction cost. Typically, to liquefy 1 kg of hydrogen, ∼12 kWh of electricity is required [21], [22]. Proportionally, this value is converted to the mass flow rate involved for each configuration and multiplied for the cost of the electricity consumed [23]. The outlet current lead is fully copper and uses hydrogen that must be warmed anyway; thus, both CAPEX and OPEX are negligible relative to the HTS inlet lead. As for the tanks, current-lead selection is posed as a linear programming problem:

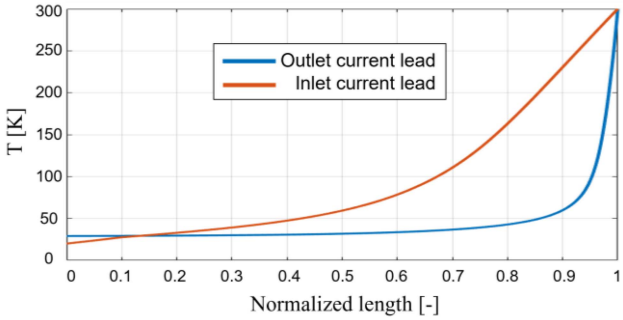

Fig. 5. Thermal profile for the selected inlet and outlet current leads.

- **Inlet lead:** The objective is the Equivalent Annual Cost, expressed in (7), with H as the time horizon considered and r the discount rate.

$$EAC=\frac{r\cdot\left(1+r\right)^H}{\left(1+r\right)^H-1}\cdot CAPEX+OPEX_{annual} \tag{7}$$

Constraints are on the stabilizer cross-section A_{stab}≤450 mm^2 (limit set by the melt-time criterion for copper), and parasitic heat to the cable Q_{cold}≤150 W, considered as negligible with respect to the ∼60 kW steady load along the cable (2 W/m × 30 km for copper).

- **Outlet lead:** Since costs are not considered, the selected configuration is the one that minimizes Q_{cold} (Fig. 5).

TABLE III
SUMMARY OF OPTIMA CURRENT LEADS

	L_{total} $[mm]$	L_{tapes} $[mm]$	$D_{conductive}$ $[mm]$	$D_{HTS}[mm]$	N_{tapes}	$\dot{m}_{H_2}$ $\left[\frac{g}{s}\right]$	$\dot{Q}_{in,cable}$ $[W]$	$CAPEX$ [€]	$OPEX$ $\left[\frac{€}{yr}\right]$
Inlet	400	40	30	25	14	0.2	147.5	~1300	~6000
Outlet	500	0	30	0	0	1 (@29K)	14.6	Negligible	0

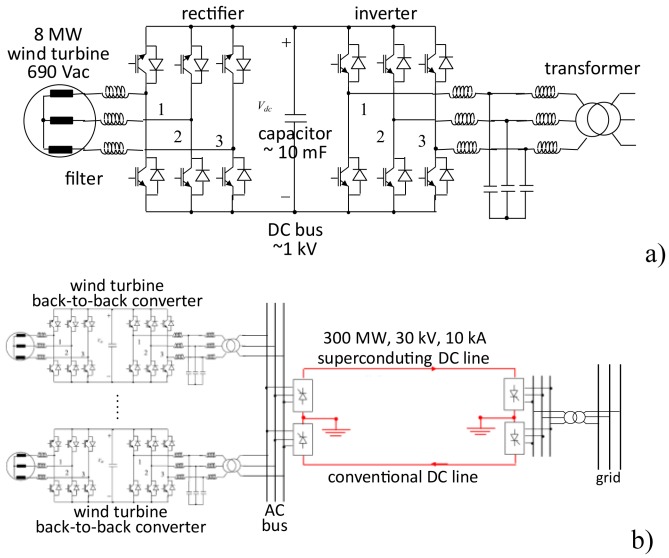

Fig. 6. Electrical layout (a) wind turbine generator with back-to-back converter (b) grid connection of the wind farm.

The resulting design values for both leads are reported in Table III, with the corresponding thermal profiles shown in Fig. 5: note that, for the inlet current lead, the selected solution does not coincide with the absolute minimum cold-end (parasitic) heat, as the additional constraints in the optimization influenced the optimum. This is a deliberate trade-off: the accepted 150 W inleak is <1% of the SCEP's external heat load (∼60 kW, ≈0.25%) and is therefore negligible at the system level.

III. GRID CONNECTION

A possible layout of the wind-farm electric grid can be based on a wind turbine back-to-back converter. This configuration allows variable-speed operation of the wind turbine, maximizing aerodynamic efficiency and providing independent control of active and reactive power. Generally, it improves power quality and enhances grid stability. The layout of the wind turbine back-to-back converter is shown in Fig. 6. A 8 MW, 690 V_{AC} wind turbine generator is selected [24], [23]. In total, about 38 wind-turbine generators will be installed. The turbine is connected to the DC-bus through an AC–DC converter, and the DC voltage on the bus is then converted back to AC using a DC–AC inverter. In the DC-bus, a ∼10 mF capacitor is added to stores and stabilizes the energy between the two converters. Filters and capacitances for reducing the reactive power are included before the connection to the transformer [25] [26], which is connected to the AC bus. An AC-DC converter with neutral point, see Fig. 6b, connects the AC bus to the 30 kV DC transmission line. The transmission line consists of a DC superconducting cable and a conventional DC cable. More details about the layout of the grid and the cable are described in [2], [4] and [6]. The transmission line is connected to the grid through a neutral-point inverter and a transformer. For the medium-voltage range considered, the CAPEX of the converter stations is estimated at ≈20–30 M€ [26].

TABLE IV
AUXILIARIES CAPEX SUMMARY

Auxiliary component	Tanks	LH_2-pump	Electric stations
Cost [M€]	0.6	0.05	20

IV. ECONOMICAL ASSESSMENT ON THE SCEP COST

A preliminary estimate of the capital costs of the superconducting cable is about 1.0 M€/km. This includes the following items [27]:

- MgB2 wires, unit price 7 €/m, total price ∼0.3 M€/km
- Copper wires, unit price 7 €/kg, total price 10 k€/km
- Polypropylene lapped paper (PPLP), unit price 10 €/kg, total price ∼2 k€/km
- Cabling of the SC cable, unit price ∼0.5 M€/km

Other capital costs related to the cable include the cryostat, with an estimated price of about 0.5 M€/km. This increases the cost of the cable to about 2.0 M€/km. The assessment of the cost related to the laying and maintenance of the line, current leads, and other operating costs is still ongoing. For a 30 km link, the cable CAPEX is estimated at ∼60 M€. Auxiliary CAPEX is summarized in Table IV. The LH_2-pump cost is referenced to the CRYOSTAR's Subtran series [28], while the current-lead CAPEX is neglected relative to the other auxiliaries. As for operating costs, a robust estimate could not be produced within the present scope due to data unavailability. Aggregating auxiliary items with the cable CAPEX yields a total of ∼80 M€, of which auxiliaries account for ∼25% . Within this auxiliary share, cryogenic auxiliaries contribute only ∼3% , with the dominant cost attributed to grid-connection/conversion infrastructure.

V. CONCLUSION

This work presented the sizing of the auxiliary subsystems (cryogenic tanks, current leads, LH_2 pump and grid interfaces) for an LH_2-cooled superconducting cable, followed by a cost assessment. The optimal layout adopts 150 m^3 tanks both upstream and downstream, with a combined CAPEX of ∼600 k€. The inlet current lead is a hybrid (Cu + REBCO HTS) cooled by 0.2 g/s of hydrogen vapor; the outlet lead is fully resistive (Cu) cooled by 1 g/s. In both cases, lead CAPEX is negligible relative to the

cable. The LH_2 pumping system, sized for the required hydraulic conditions, contributes $\sim$50 k€. Grid-connection hardware is the dominant auxiliary cost item, accounting for 20–30 M€. Under these assumptions, auxiliaries correspond to $\sim$25% of the overall system CAPEX. A deeper assessment of the SCEP should address: (i) a rigorous estimation of system operating costs; (ii) the sizing and cost modeling of the liquefaction unit and its integration with the pipeline; and (iii) a more detailed end-to-end plant design of the overall facility.

ACKNOWLEDGMENT

This article reflects only the authors' views and opinions, and the Ministry cannot be considered responsible for them.

REFERENCES

[1] Terna, "Dati statistici sull'energia elettrica in Italia 2023," 2003.
[2] L. Savoldi, A. Balbo, C. E. Bruzek, G. Grasso, M. Patti, and M. Tropeano, "Conceptual design of a SuperConducting energy pipeline for LH2 and power transmission over long distances," *IEEE Trans. Appl. Supercond.*, vol. 34, no. 3, May 2024, Art. no. 5400805.
[3] N. Magnusson et al., "SCARLET – A European effort to develop HTS and MgB_2 based MVDC cables," *IEEE Trans. Appl. Supercond.*, vol. 34, no. 3, 2024, Art. no. 5400205.
[4] M. Bracco et al., "Design of a submarine 30-km MgB_2 cable for the combined transfer of 0.3 GWe and LH_2 from offshore plants to the Ravenna port," *IEEE Trans. Appl. Supercond.*, vol. 35, no. 5, 2025, Art. no. 5400906.
[5] J. Nagamatsu et al., "Superconductivity at 39 K in magnesium diboride (MgB_2)," *Nature*, vol. 410, no. 6824, pp. 63–64, 2001.
[6] L. Cavallucci et al., "Analysis of electric fault in a MV DC MgB_2 transmission line cooled by liquid hydrogen," presented at EUCAS, Porto, Portugal, Sep. 21-25, 2025.
[7] L. Savoldi et al., "Analysis of the evolution of accidental transients in the cooling of a MgB_2-LH2 hybrid power cable," presented at the 17th Eur. Conf. Appl. Supercond., Porto, Portugal, Sep. 21-25, 2025.
[8] M. Kang et al., "Experimental investigation of thermal stratification in cryogenic tanks," *Exp. Thermal Fluid Sci.*, vol. 96, pp. 371–382, 2018.
[9] S. P. Kumar et al., "Influence of surface evaporation on stratification in liquid hydrogen tanks of different aspect ratios," *Int. J. Hydrogen Energy*, vol. 32, no. 12, pp. 1954–1960, 2007.
[10] L. V., "Interviewee," in *Request for a Quotation of Different Cylindrical Tank (Linde)*. [Interview], Sep. 2025.
[11] A. Alekseev, "Hydrogen liquefaction," in *Hydrogen Science and Engineering: Materials, Processes, Systems and Technology*. Weinheim, Germany, Wiley-VCH, 2016, pp. 733–761.
[12] D. Avcı et al., "Optimized superconducting MgB_2 joint made by IMD technique," *Supercond. Sci. Technol.*, vol. 36, 2023, Art. no. 075004.
[13] M.-K. Wu et al., "Superconductivity at 93 K in a new mixed-phase Y-Ba-Cu-O compound system at ambient pressure," *Phys. Rev. Lett.*, vol. 58, no. 9, pp. 908–910, 1987.
[14] M. N. Wilson, "Current supply," in *Superconducting Mangnets*. London, U.K.: Oxford Univ. Press, 1983, pp. 256–273.
[15] R. Heller, "Predictive 1-D thermal-hydraulic analysis of the prototype HTS current leads for the ITER correction coil," *Cryogenics*, vol. 80, no. 3, pp. 325–332, 2016.
[16] A. Ballarino, "Current leads, links and buses," in *Proc. CERN Yellow Rep.: Sch. Proc.*, Geneva, Switzerland: CERN, 2015.
[17] J. Lu et al., "Thermal conductivity of REBCO tapes with different stabilizers from 4.2 to 200 K," in *IOP Conf. Ser.: Mater. Sci. Eng.*, vol. 1327, 2025. Art. no. 012226.
[18] N. J. Simon et al., "Properties of copper and copper alloys at cryogenic temperatures," in *NIST Monograph,* vol. 177. Washington, DC, USA: U.S. Government Printing Office, 1992.
[19] R.D. McCarty et al., "Selected properties of hydrogen (engineering design data)," National Bureau of Standards, U.S. Dept. of Commerce vol. 168. Washington, DC, USA, Feb. 1981.
[20] K. Wang et al., "Advances in second-generation high-temperature superconducting tapes and their applications in high-field magnets," *Soft Sci.*, vol. 2, no. 12, pp. 1–28, 2022.
[21] K. Ohlig et al., "The latest developments and outlook for hydrogen liquefaction technology," in *Proc. Cryogenic Eng. Conf.*, 2014, pp. 1311–1317.
[22] M. Gardiner et al., "Energy requirements for hydrogen gas compression and liquefaction as related to vehicle storage needs," in *Hydrogen and Fuel Cells Program*. Washington, DC, USA: U.S. Department of Energy, 2009.
[23] 2024. [Online]. Available: https://www.agnespower.com/eolico-offshore-adriatico/
[24] L. Quéval et al., "Back-to-back converter design and control for synchronous generator-based wind turbines," in *Proc. Int. Conf. Renew. Energy Res. Appl.*, Nagasaki, Japan, 2012, pp. 1–6.
[25] S. M. Muyeen, R. Takahashi, and J. Tamura, "Operation and control of HVDC-connected offshore wind farm," *IEEE Trans. Sustain. Energy*, vol. 1, no. 1, pp. 30–37, Apr. 2010.
[26] P. Bresesti, W. L. Kling, R. L. Hendriks, and R. Vailati, "HVDC connection of offshore wind farms to the transmission system," *IEEE Trans. Energy Convers.*, vol. 22, no. 1, pp. 37–43, Mar. 2007.
[27] L. Cavallucci et al., "Optimization procedure to design a DC transmission line with MgB_2 wires in liquid hydrogen," *IEEE Trans. Appl. Supercond.*, vol. 35, no. 5, 2025, Art. no. 5400205.
[28] N. W., "Interviewee," in *Request for a Quotation of the LH2 Subtran pump (Cryostar)*. [Interview], Sep. 2025.